IEEE Access
Multidisciplinary | Rapid Review | Open Access Journal

Received September 9, 2021, accepted September 29, 2021, date of publication October 11, 2021,
date of current version November 8, 2021.

Digital Object Identifier 10.1109/ACCESS.2021.3117375

Dependancy of Three Phase Induction Motor Derating Aspects on Complex Voltage Unbalance Factor: A Calorimetric and Finite Element Simulation Study

PATHUM SUDASINGHE[1], (Member, IEEE), UPULI JAYATUNGA[1], (Senior Member, IEEE), PHILIP COMMINS[2], (Member, IEEE), JEFF MOSCROP[3], (Member, IEEE), AND SARATH PERERA[3], (Senior Member, IEEE)

[1]Department of Electrical Engineering, University of Moratuwa, Katubedda, Moratuwa 10400, Sri Lanka
[2]School of Mechanical, Materials, Mechatronics and Biomedical Engineering, University of Wollongong, Wollongong, NSW 2522, Australia
[3]School of Electrical Computer and Telecommunications Engineering, University of Wollongong, Wollongong, NSW 2522, Australia

Corresponding author: Pathum Sudasinghe (spms677@uowmail.edu.au)

ABSTRACT It is well known that three-phase induction motors have to be derated in the presence of supply voltage unbalance (negative sequence) exceeding a stipulated limit of 1% based on several widely used standards. Generally, voltage unbalance limits are decided based on the magnitude of negative sequence voltage unbalance factor which is quantified as the ratio of negative sequence voltage to positive sequence voltage. However, a specified voltage unbalance magnitude can arise as a result of numerous possibilities of the three phase supply voltages. Therefore, it is hypothesised that the current derating curve, which defines a derating factor that is dependent on the magnitude of the voltage unbalance, is not optimal and may not be economical and/or safe for some voltage unbalance conditions. To examine the validity of this hypothesis, modelling and experimental validation need to be carried out considering motor losses and temperature rise which are the main factors that help determine the derating factor of an induction motor. Realising these requirements, the emphasis of this study is to examine the dependency of losses, temperature rise and torque oscillations of a three-phase induction motor on the complex nature of voltage unbalance through calorimetric and finite element simulation-based studies. The outcomes are expected to assist in the development of suitable derating factors.

INDEX TERMS Complex voltage unbalance factor, double chamber calorimeter, finite element simulations, temperature rise, three-phase induction motor derating, torque ripple, voltage unbalance.

I. INTRODUCTION

Voltage Unbalance (VU) is a common and unavoidable condition in power systems which arises for many reasons that are well documented [1]. Mains connected three-phase induction motors (IMs) are considered as the main work horse in industrial applications and are adversely affected by supply VU. The main adverse effect of supply VU on three-phase IMs is the excessive temperature rise caused by the increased and unevenly distributed losses, leading to the degradation of motor insulation life [2]. Not only the loss of life, but also the increased noise and vibration levels, reduced efficiency, and reduced output torque are other consequences of VU. The increased noise and vibration levels are attributed to the double frequency harmonic in electromagnetic torque which is proportional to the magnitudes of the positive and negative sequence voltages [3].

The adverse effects of VU on IMs have been investigated since the 1950s, which has resulted in the development of derating factors such that the temperature rise at hotspots does not exceed the limiting values for the safe operation of motors in the presense of supply source unbalance [1], [2], [4]. The NEMA standard [5] recommends derating three-phase IMs with the help of a derating curve which is based on the

The associate editor coordinating the review of this manuscript and approving it for publication was R. K. Saket.

Percent Voltage Unbalance (PVU), as defined in (1). A similar guideline was introduced by IEC in [3] which provides the derating factors based on the magnitude of Complex Voltage Unbalance Factor (CVUF) as defined in (2).

$$\text{PVU} = \frac{\text{Maximum line voltage deviation from average line voltage magnitude}}{\text{Average line voltage magnitude}} \quad (1)$$

$$\text{CVUF} = \frac{\text{Negative sequence voltage}}{\text{Positive sequence voltage}} = VUF\angle\theta \quad (2)$$

There are an unlimited number of combinations of phase voltages which can give rise to the same PVU or CVUF magnitude. Each set of combinations can lead to different motor performances in relation to losses, vibration, and temperature rise [2], [4]. Thus, the positive sequence voltage magnitude is another critical quantity that influences the losses and temperature rise of IMs, and hence has an influence on the derating that should be applied for safe and economical operation of IMs running under VU conditions.

Furthermore, a small change in VU can cause a significant current unbalance resulting in disproportionate unbalanced currents to flow in the three phases. Thus, the Complex Current Unbalance Factor (CCUF), which is the ratio of the negative sequence current to the positive sequence current, can also be used to describe the severity of the impact of VU on IMs. In particular, CCUF angle was found to be a critical parameter. When the positive and negative sequence currents corresponding to a particular phase winding are in phase (i.e. the angle of CCUF $= 0°$), the relative phase current in that particular phase winding results in a large localised loss density. Conversely, for 180° out-of-phase sequence currents (angle of CCUF $= 180°$), the effects of VU are less severe than those of the former case [6].

Therefore, it is essential to study the impact of the magnitude of VU, angle of CCUF, and positive sequence voltage on the variation of losses, temperature rise, and vibration level of three-phase IM operating under supply VU. Thus, an informed understanding can be developed on the required derating instead of using a single generalised derating curve. While theoretical studies can be carried out to supplement the above differences [2], the aim of the work presented in this paper is to analyse the impact of such influential factors on motor derating while examining their variability on motor terminal conditions. The investigations cover experimental procedures using an advanced calorimetric platform as well as detailed finite element (FE) simulations in Altair Flux 2D platform.

Experimental investigations are essential for analysing the effects of VU on three-phase IM derating owing to the complex nature of its electromagnetic and thermal behaviour under supply VU. Calorimetry is the most accurate measurement method which can be used to measure electrical machine losses [7]. However, comprehensive experimental studies on three phase induction motor testing for losses and torqure-speed oscillations under unbalanced supply source conditions are hardly found in the literature. Further, due to the time and resource requirements of the experimental measurements, it is not practically possible to carry out experimental investigations on all possible different voltage unbalance scenarios. Therefore, a numerical model whose accuracy was verified against the experimental results is vital in this study. FE numerical modelling platforms offer the capability to model the electromagnetic and thermal behaviour of electrical machines with a higher accuracy compared to the conventional electromagnetic and thermal models [8]. However, owing to the complexities associated with both magnetic and thermal models of electrical machines, they are modelled in two different independent FE platforms. To improve the accuracy of the losses, temperature and torque simulated with FE models, the interaction between electromagnetic and thermal properties can be incorporated in the simulation with electro-thermal co-simulations by performing several iterations of simulation with shared outputs between electromagnetic and thermal platforms. However, these co-simulation techniques have not been widely used in the literature because of their complexity and higher computer resource requirements.

This paper presents a comprehensive sensitivity analysis of the factors influencing the derating of three-phase induction motors using both experimental and numerical modelling platforms. Experimental investigations were carried out using an improved version of an advanced air-cooled double-chamber calorimeter (DCC) developed with a higher measurement accuracy and reduced measuring time compared to the calorimeters detailed in the literature [9]. This calorimeter platform was then improved into an electrical machine testing platform which can be used to examine their losses, temperature variations, and torque and speed oscillations under different network conditions. Not only the electromagnetic behaviour, but also the thermal behaviour of the test motor, including the interaction between magnetic and thermal domains, have been modelled in the FE platform to verify and extend the experimental results. Furthermore, this study presents a sensitivity analysis of CVUF and positive sequence voltage on the steady-state torque ripple of three-phase induction motors which has not been studied in detail in the literature.

The remainder of the paper is organised as follows. Section II describes the detailed design of the experimental platform and the FE simulation model. Section III describes the experimental methodology for the use of the calorimetric test platform to evaluate the performance of a three-phase IM operating under VU conditions. The results of the *study* are presented in Section IV, followed by the conclusions in Section V.

II. EXPERIMENTAL AND SIMULATION PLATFORMS

A. ADVANCED CALORIMETRIC PLATFORM

Calorimeters are widely used to measure the losses of electrical machines owing to the higher measurement uncertainties associated with conventional efficiency measurement techniques. Different calorimeter configurations were introduced

in the literature [7] to address the limitations associated with the calorimeter technology, such as the complexity and time-consuming nature of the measurements.

An air-cooled double-chamber calorimeter was designed to facilitate the testing of motors with a rated output power of up to 3 kW, as shown in FIGURE 1. Details of the design are presented in Appendix A. The motor (device under test) is located in one chamber (chamber 1), and the reference heater (the known heat source) is located in the other chamber (chamber 2). Air flow was maintained through both chambers using an inlet fan, and the temperature rise through each chamber was measured separately. Heat is transferred from both the motor and the heater through conduction, convection, and radiation. Although the calorimeter is designed to experience negligible radiation heat leakage, it is not possible to eliminate conduction heat leakage which is calculated for each chamber, as described in Appendix B. These results are used to calculate the heat generated by the motor, as given in (3) [9], where q_{cond} is the conduction heat leakage, C_p is the specific heat capacity of air, and ΔT is the temperature rise, while subscripts 1 and 2 refer to the respective chambers relevant to each parameter.

$$P_{motor} = (P_{heater} - q_{cond2}) \times \left(\frac{C_{p1}\Delta T_1}{C_{p2}\Delta T_2}\right) + q_{cond1} \quad (3)$$

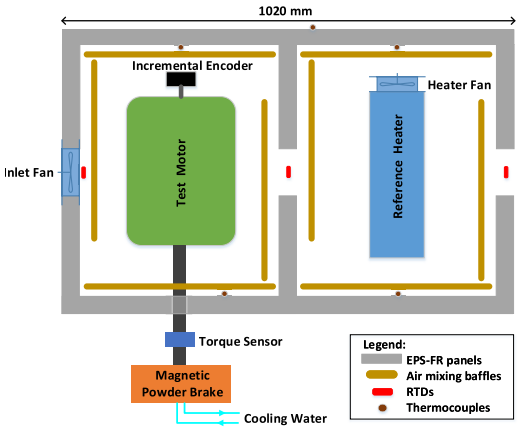

(a) Top view

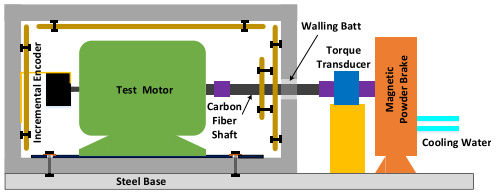

(b) Side View

FIGURE 1. **Double chamber calorimeter test platform.**

To improve the accuracy of the loss measurement, the humidity of air in each chamber was measured to determine C_{p1} and C_{p2} as the specific heat capacity of air depends on both humidity and temperature which has not been addressed in previous studies [9]. As heating within the calorimeter is a 'sensible heating' process, the dew point of the air remains unchanged throughout. Therefore, the average humidity values of each chamber can be determined by measuring the dew point of the inlet air using a dry and wet bulb hygrometer and a psychometric chart. With the known humidity and temperature, C_{p1} and C_{p2} can be determined using the specific heat capacity curves given in [10].

Owing to the complex nature of the wall design, the thermal conductivity of the walls of the finished calorimeter is not equal to the thermal conductivity of the EPS. Hence, to improve the accuracy of the measurements, a series of tests were conducted to estimate the average thermal conductivity of the walls as detailed in Appendix B. The results confirmed that the conduction heat leakage of the chambers can be estimated with a maximum discrepancy of 2 % using this method.

Calibration tests were carried out to establish a suitable air flow rate and a reference heater power level to improve the accuracy of the measurements. The calibration tests also determined the limits and the associated errors in the measurements of the experimental setup. It was found that the errors were relatively large for lower airflow rates, as a result of poor air mixing and highly uneven temperature distribution within the chambers. The measurement errors for flow rates of 40 L/s and 50 L/s were found to be 1.2 % and 2.5 %, respectively, with 95 % of confidence. In addition, the experimental results indicated that the reference heater power should be close to the measured loss in order to achieve better accuracy. The variation in the measurement error for different power levels of the calibration heater with an air flow rate of 40 L/s is shown in FIGURE 2 using box and whisker plots. TABLE 1 summarises the performance of loss measurement using the calorimeter platform.

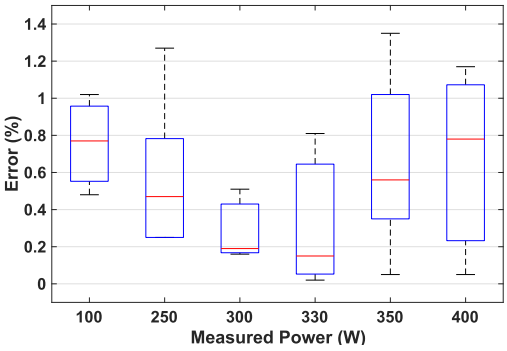

FIGURE 2. **Calibration test results for reference heater power of 300 W at 40 L/s air flow rate.**

Another requirement of the test setup was to measure the electromagnetic torque produced by the motor, including its ripple components, especially that is caused by the supply voltage unbalance. This requires a constant torque load that is independent of speed. If the load is speed dependent, then the mechanical behaviour of the system would be much more complicated and would be difficult to study the torque oscillation owing to the supply voltage unbalance. Therefore,

TABLE 1. Characteristics of the loss measurements in the advanced calorimeter measurement platform.

Parameter	Condition 1	Condition 2
Air flow rate (L/s)	40	50
Measurement range (W)	0 - 400	0- 600
Maximum error (%)	1.2	2.5
Test duration (hrs)	3	3

a magnetic powder brake was used as the load, where the torque depends only on its DC excitation current, irrespective of the speed of the shaft [11]. The selected powder brake can produce up to 100 N m of load torque is rated at 3 kW. The key details of the sensors and measuring instruments used in the test platform are summarised in TABLE 4 in Appendix A.

B. FINITE ELEMENT SIMULATIONS

The main objective of the FE simulations is to build an accurate numerical model to predict the losses and temperature rise of the motor windings for a given voltage unbalance at the motor terminals, as it is not possible to experimentally evaluate them for each voltage unbalance condition. The test motor was modelled on the Altair Flux 2D FE simulation platform, as it was not possible to evaluate the losses and temperature rise of the test motor for each voltage unbalance condition owing to the longer time required for one test. Losses of the motor were evaluated with 2D electromagnetic transient application as it provides better results compared to 2D steady state simulations for unbalanced systems.

The thermal behaviour of the motor is modelled in the a 2D steady-state thermal application and used to evaluate the temperature rise of the windings with the losses calculated from electromagnetic application as inputs. Owing to the interdependency of the winding temperature, magnetic losses, and the material properties of the motor, a co-simulation between electromagnetic and thermal platforms was used to obtain the final result. The use of the co-simulation technique improves the accuracy of the results but considerably increases the simulation time. It is vital to model the correct geometry of the motor for the FE simulations to achieve a better accuracy. However, because the motor internal geometry data are not readily available, a sacrificial motor of the same type was cut in half and used to measure the geometric details and establish material properties as described in [2]. The stator and rotor cores were modelled as laminated magnetic non-conducting regions of M-36 electrical grade steel. The 2D geometry with the mesh used for the simulations is shown in FIGURE 3 where quarter symmetry is employed. To simulate the skin effect, rotor bars were modelled as solid conductor regions of die-cast aluminium with a resistivity of $4.9 \times 10^{-8}\,\Omega\,\mathrm{m}$. Losses of the motor for different VU conditions under test were established through transient simulations on Altair Flux 2D and the Bertotti loss model with the model coefficients as given in given in Table 2 was used to estimate the core loss of the motor. Considering the simulation time and resources required, the rotor skew was not modelled for electromagnetic simulations for loss estimation. Friction and windage losses were included in the total loss measurement obtained from the DCC. However, friction and windage losses are proportional to the speed and the average speed remains nearly constant for a given load condition irrespective of the voltage unbalance condition at the motor terminal. Therefore, the friction and windage losses were modelled as a constant of 35.5 W in FE simulations and the value was experimentally calculated according to [12].

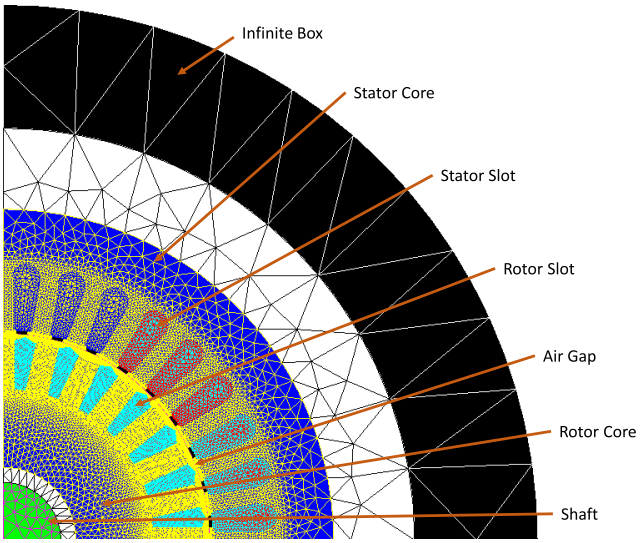

FIGURE 3. 2D geometry of FE model with the mesh.

TABLE 2. Coefficients of Bertotti model for M-36 electrical grade steel.

Coefficient	Value
K_{hys}	$306.5\,\mathrm{W\,s\,T^{-2}\,m^{-2}}$
K_{class}	$4\,500\,000\,\mathrm{S\,m^{-1}}$
K_{exc}	$0.61\,\mathrm{W\,T^{-1.5}\,s^{-1.5}\,m^{-3}}$

Limitations of the simulation model arise from estimation of the electromagnetic and thermal properties of materials and other general material properties, which could differ from the actual values due to the anormalies associated with the manufacturing process.

Experimental results are compared with the FE simulation results in Section IV.

III. STUDY ON LOSS, TEMPERATURE RISE AND TORQUE/SPEED HARMONICS

The aforementioned test platform and FE simulations were used to measure and analyse the losses, speed, and torque pulsations of the test motor operating under different VU conditions ($|\mathrm{CVUF}| = 1\%$ to 5%). The name plate data of the 2.2 kW, 400 V squirrel cage three-phase IM used are given in TABLE 3. A three phase IM with a die cast aluminium rotor was used as it is the most commonly available and the widely

used rotor type in the industry owing to many advantages such as cost effectiveness. The test motor was energised in a star configuration in order to measure the correct phase voltage of each winding. However, the star point is kept ungrounded to minimise the zero sequence currents, as the main focus of the study is on negative sequence voltage unbalance.

Normally, the temperature rise of the windings is the most critical factor that governs the life of a motor. Premature motor failures occur due to the increased temperature rise of windings caused by unevenly distributed losses in the three phases. Therefore, Type T thermocouples were placed in the middle slot of each stator phase winding pole of the test motor to measure the maximum steady-state temperature rise. A thermal paste with a thermal conductivity of 3.8 W/mK was used to increase the thermal bond between the winding and the thermocouple.

Tests were carried out under various VU conditions falling under two main categories as given below, to examine the effect of the magnitude of VU, the magnitude of the positive sequence voltage V_{pos} and the angle of CCUF.

CAT I - |CVUF| ranging between 1 % - 5 % having $V_{pos} = 230$ V

CAT II - V_{pos} ranging between 220 V - 240 V having |CVUF| of 4 %

For each CAT I and CAT II, VU conditions corresponding to the two angles of CCUF equal to 0° and 180° were considered where the initial results demonstrated that the difference between the angle of CCUF and the angle of CVUF is nearly the same for a given loading level. Therefore, the VU conditions were set to obtain the corresponding angles of CVUF equal to 15° and −165° were considered to correspond to CCUF angles of 0° and 180° respectively, under the loading level used in the tests. A California Instruments MX45 programmable power source was used to generate the unbalanced supply voltage conditions for the experiments. Voltage unbalance conditions with simultaneous unbalance in both voltage magnitude and phase were considered in this study.

Each test was carried out with the motor loaded to 85 % of the full load in order to safeguard the motor from premature failure which can jeopardise the remaining experimental work (However, a similar methodology can be applied to test the motor in other loading levels as well). The torque, speed, power loss, winding temperatures, and resistance of the windings were recorded once the system had reached the thermal steady state, where the variation of temperatures within a 20 minute period was observed to be below 0.1 °C [10]. The typical duration of a single test was approximately 5 hours, which can be reduced to 3 hours by externally heating the inlet air at the beginning of the experiments until the temperature reached the required level.

IV. RESULTS

A. VARIATION OF LOSSES

Loss Increase Rate (LIR) as defined in (4) is used to analyse the nature of variation of losses of the motor under different VU conditions.

$$\text{LIR} = \frac{\text{Losses under unbalanced condition}}{\text{Losses under balanced condition}} \tag{4}$$

TABLE 3. 2.2 kW, 4-pole, 400 V, 50 Hz motor data.

Parameter	Value
Rated speed	1440 rpm
Rated Current (I_n)	4.54 A
Rated Torque (T_n)	14.6 N m
No load current	2.6 A
Locked rotor current	37.7 A ($8.3I_n$)
Locked rotor torque	57 N m ($3.9T_n$)

FIGURE 4a compares the variation of LIR obtained from experimental measurements and simulations with the magnitude of CVUF for the VU conditions corresponding to the two cases: CCUF = 0° and 180°, where the positive sequence voltage is kept constant at 230 V. This shows that the LIR sharply increases with the magnitude of CVUF (i.e. LIR sharply increases with the negative sequence voltage), and it can be different between the two cases even though the |CVUF| level is identical. FIGURE 4b shows the variation of LIR with the positive sequence voltage for the VU conditions corresponding to the two cases mentioned above, where the magnitude of the CVUF is 4 %. It can be observed in general that LIR is higher, corresponding to the case where $\theta_{CCUF} = 0°$ in comparison to the same when $\theta_{CCUF} = 180°$. The variation of LIR with positive sequence voltage (220 V – 240 V) shows a minimum at around the rated voltage of 230 V. This behaviour can be explained by considering the manner in which core losses and the copper losses of the motor vary with the positive sequence voltage [2]. The core losses are dominated by those on the stator and will be proportional to the positive sequence voltage, whereas the rotor core losses can be disregarded considering the very low frequency of the rotor flux. The rotor and stator copper losses will exhibit an opposite behaviour compared to that of core losses, where they will be higher at lower positive sequence voltages compared to those at higher positive sequence voltages. Thus, the two contrasting variations associated with core and copper losses lead to a local minimum observed at around the rated voltage of the motor. Furthermore, both experimental and simulation results demonstrate a similar variation in the LIR indicating close alignment.

B. TEMPERATURE RISE

Unevenly distributed losses lead to hotspots in stator windings and is the main factor governing the effect of VU on the insulation life. The maximum percentage temperature rise (PTR) was calculated using (5), from the recorded temperature data of all thermocouples in the stator slots.

$$\text{PTR} = \frac{T_{max,VU}}{T_{bal}} \tag{5}$$

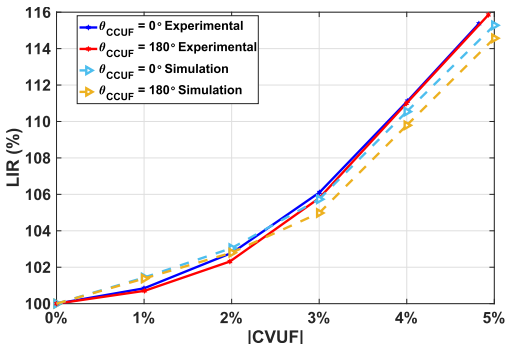

(a) $V_{pos} = 230\,\text{V}$

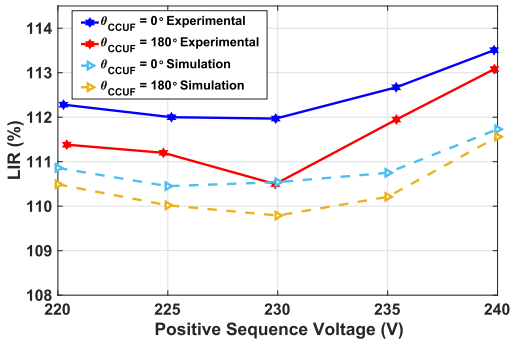

(b) |CVUF| = 4 %

FIGURE 4. Variation of LIR of the motor operating at 85% full load.

where,

$T_{max,VU}$ - Maximum temperature rise of any winding under VU

T_{bal} - Temperature rise of the same spot under balanced supply and at 85% mechanical loading

FIGURE 5a shows the variation in the maximum PTR with the magnitude of CVUF for the VU conditions corresponding to the two cases: CCUF = 0° and 180°, where the positive sequence voltage is kept constant at 230 V. Further, it can be observed that the maximum PTR sharply increases with the magnitude of CVUF and is different for the two cases for identical |CVUF| levels. Furthermore, it can be observed that a relatively higher temperature rise of the winding occurs for the case where $\theta_{CCUF} = 0°$ compared to the same where $\theta_{CCUF} = 180°$.

FIGURE 5b shows the variation of the maximum PTR with the positive sequence voltage for VU conditions corresponding to the two cases of θ_{CCUF} where the magnitude of CVUF is maintained at 4 %. It can be clearly observed that the maximum PTR is greater when $\theta_{CCUF} = 0°$ in comparison to the case where $\theta_{CCUF} = 180°$ for the chosen |CVUF| of 4%. When $\theta_{CCUF} = 0°$, a larger unbalanced current is confined to one phase (Phase A), and the temperature of that phase has increased considerably owing to the higher density of the increased loss. However, the VU condition corresponding to $\theta_{CCUF} = 180°$ caused an increase in current in two phases (Phases B and C), where the I^2R loss increases in both phases, but the density of the increased loss is much smaller compared to the case corresponding to $\theta_{CCUF} = 0°$. Therefore, it is not the total loss, but the temperature rise is the most relevant factor that determines the derating levels for safe motor operation.

Furthermore, it can be observed from both FIGURE 5a and FIGURE 5b that the simulated maximum PTR is slightly lower than the experimental values. This is due to the use of only one iteration of electromagnetic and thermal FE co-simulations.

Derating factors for each case can be measured experimentally by loading the motor under each VU condition until the maximum PTR reached 100 %. However, FIGURE 5b shows that the required derating factor for |CVUF| of 4 % for this motor is higher than 0.85 as the maximum PTR for all cases is less than 100 %. However, NEMA recommended derating factor is 0.825. Therefore, it seems uneconomical to derate the motor to the NEMA derating level for different motor terminal VU conditions which leads to |CVUF| of 4 %.

Slight deviations can be observed in the simulation results compared to the experimental results in both FIGURE 5a and FIGURE 5b. This could be attributed to the limitations of the FEA model detailed in Section II-B. However, a similar trend can be observed in the variation of LIR and PTR in both simulation and experimental results which is the main focus of this study.

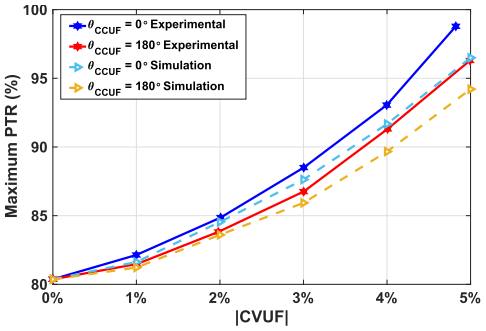

(a) $V_{pos} = 230\,\text{V}$

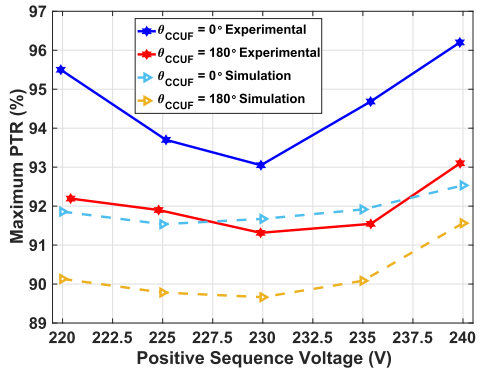

(b) |CVUF| = 4 %

FIGURE 5. Variation of the percentage temperature rise (PTR) of the motor operating at 85% full load.

C. TORQUE AND SPEED OSCILLATIONS

FIGURE 6a shows the time and frequency domain torque/speed signals observed during the motor operation

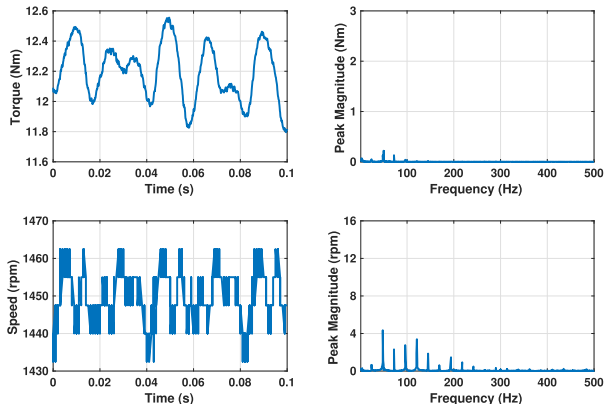

(a) Balanced supply conditions

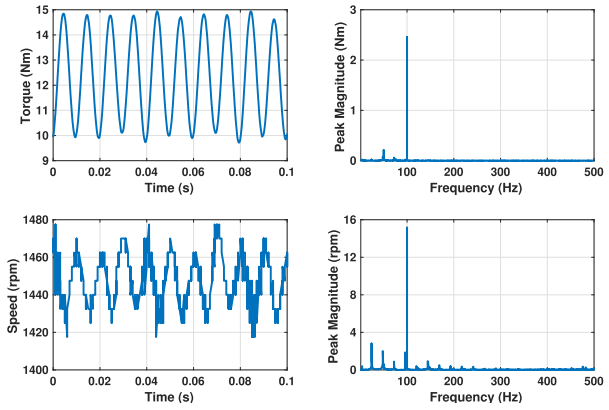

(b) CVUF = 5 %∠15°V_{pos} = 230 V

FIGURE 6. Torque, speed signals and their harmonics of the motor operating at 85% full load under balanced and unbalanced supply conditions.

under balanced supply conditions at 85 % of the loading level. Relatively small torque and speed harmonics can be observed during the balanced operation of the motor, which can be attributed to the space harmonics and mechanical characteristics of the coupled motor-load system.

FIGURE 6b shows the time domain and frequency domain torque/speed signals observed during the motor operation under 5 % |CVUF| at 85 % of the loading level. A significant increase in the double frequency torque and speed harmonic components was observed when the motor is operating with unbalanced voltages.

FIGURE 7a shows the variation in the magnitude of the double frequency torque and speed harmonics as a percentage of the same under balanced supply conditions with |CVUF|, while the motor is operating with a positive sequence voltage of 230 V and loaded at 85 %. This shows that there is a linear relationship between the |CVUF| and the magnitude of the double frequency torque and speed harmonics. This variation was observed to be independent of whether $\theta_{CCUF} = 0°$ or $\theta_{CCUF} = 180°$.

FIGURE 7b shows the variation in the magnitude of the double frequency torque and speed harmonics with the positive sequence voltage for the motor operating with 4 % VUF, and loaded at 85 %. It can be observed that the magnitude of the double frequency torque and speed harmonics also has a linear relationship with the positive sequence voltage.

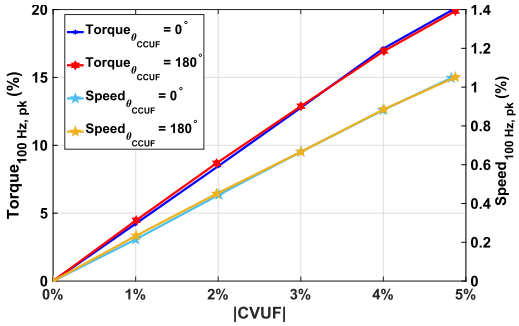

(a) V_{pos} = 230 V

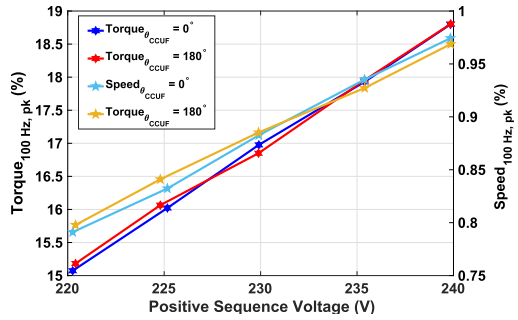

(b) |CVUF| = 4 %

FIGURE 7. Variation of the double frequency torque and speed component of the motor operating under 85% of full load (experimental results).

V. CONCLUSION

This paper presents a comprehensive study on the factors influencing the derating of three-phase induction motors using both experimental and numerical modelling platforms. The relevant IEC and NEMA standards that are currently in use, decide the level of IM derating based only on the magnitude of the VUF or PUV. However, the study outcomes reveal that the motor losses and temperature rise, thus motor derating is dependent on the complex nature of voltage unbalance. Thus, the angle of CVUF or CCUF and the positive sequence voltage should also be taken into account in determining effective derating levels for an IM. For a given VUF, the maximum temperature rise of the windings occurs when CCUF = 0° and for higher positive sequence voltages.The study outcomes indicate the requirement for more precise derating levels leading to economical benefits.

Advanced double-chamber calorimetric method presented in this study can be used to determine precise derating under different VU conditions and the variation of limits required for derating factors. Furthermore, the multi-physics finite element model presented, simulates the true to life performance of IM operation under unbalanced conditions with reasonable accuracy as validated through the experimental platform. Thus, the study provides a pathway for a generic IM derating mechanism through the finite element model

that scales the derating outcomes without carrying out time consuming and expensive experimental work.

APPENDIX A
DESIGN AND CONSTRUCTION

The air-cooled DCC was designed to facilitate the testing of motors with a rated output power of up to 3 kW, as shown in FIGURE 1. The calorimeter walls were made with 100 mm thick SL grade expanded polystyrene (EPS) panels with a thermal conductivity of 0.04 W/mK at 20 °C.

A DC axial fan maintains the airflow through both chambers. The baffles are placed as shown in FIGURE 1 to prevent the radiation heat leakage and to improve the efficiency of convection heat transfer by mixing air inside the chambers. The motor shaft is connected to the load located outside the calorimeter through a carbon-fiber tube to limit the conduction heat leakage. Carbon-fiber was selected for the shaft owing to its higher strength at elevated temperatures. The gap between the shaft and the wall of the calorimeter was filled with glass wool batts having a thermal conductivity of 0.052 W/mK. However, based on measurements, these batts led to an additional frictional loss of around 10 W.

Inlet, mid-wall and outlet air temperature measurements are the most important and sensitive measurements to establish the accuracy of a calorimeter test setup. In addition, the accuracy of the power measurement of the reference heater has a significant impact on the accuracy of the results obtained using (3).

The key details of the sensors and measuring instruments used in the test platform are summarised in TABLE 4.

TABLE 4. Measuring equipments and accuracies.

Measurement	Sensor/Equipment	Accuracy
Air temperature	4-wire Pt-100 RTD	±0.15 °C
Wall / motor winding temperature	Type T Thermocouples	±0.5 °C
Heater / motor input power	Power Analyzer	±0.1 W
Torque	20 Nm HBM Torque sensor	±0.5 %
Speed	Incremental encoder	10,000 ppr
Winding resistance	milliohm meter	±1 mΩ

APPENDIX B
MODELLING THE CONDUCTION HEAT LEAKAGE

Heat leakage through the calorimeter walls can be calculated as the sum of heat leakage through the plane slab sections, edge and corner sections using the mathematical models given in TABLE 5, where k is the thermal conductivity, A is the area of the slab section, L is the length of the edge, t is the thickness of the wall and ΔT is the temperature difference [13].

In order to improve the accuracy of the results, series of tests were conducted to estimate the average thermal conductivity of the calorimeter walls. The middle wall separating the two chambers was removed and the calorimeter was made airtight by sealing the inlet and outlet with an expanding polyurethane foam. Two heaters were placed inside the calorimeter with DC fans, as shown in FIGURE 8a. By applying a known amount of power with the heaters, the wall temperatures were measured in the steady-state using RTDs placed on the internal and external walls. According to IEC 34-2 [10], the test system can be assumed to have reached the thermal steady state when the temperature difference between measurements was less than 0.1 °C during a period of 20-30 minutes. The variation in the average thermal conductivity of the walls is shown in FIGURE 9, where T_{avg} is the average temperature of the wall.

TABLE 5. Mathematical models used to establish conduction heat leakage through walls.

Geometric Section	Formula
Slab Section	$q_{slab} = \frac{kA\Delta T}{t}$
Edge Section	$q_{edge} = 0.54kL\Delta T$
Corner Section	$q_{corner} = 0.15kt\Delta T$

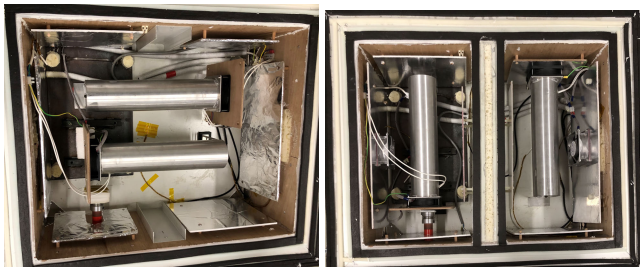

(a) (b)

FIGURE 8. Test set ups used to determine calorimeter conduction heat leakage (a) through outside walls only; (b) when operated as two chambers.

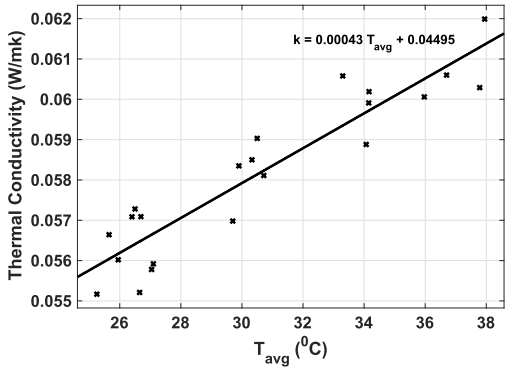

FIGURE 9. Average thermal conductivity of calorimeter walls.

A secondary test was performed to verify the accuracy of the conduction heat leakage calculations when the calorimeter was operated as two chambers at different temperatures. The middle wall was reinstalled in place with a heater in

each chamber, as shown in FIGURE 8b. Known power levels were dissipated in the heaters, and the wall temperatures were measured. The conduction heat leakage of the two chambers was calculated separately using the models given in TABLE 5 and compared with the measured power of each heater. The results confirmed that the described models can be used to calculate the conduction heat leakage of the chambers with a maximum discrepancy of 2 %.

REFERENCES

[1] A. von Jouanne, "Assessment of voltage unbalance," *IEEE Trans. Power Del.*, vol. 17, no. 4, pp. 1176–1177, Oct. 2002.

[2] P. Sudasinghe, S. Perera, P. Commins, J. Moscorp, U. Jayatunga, and P. Wadduwage, "Revisiting the effects of supply voltage unbalance on the losses of three phase induction motors," in *Proc. Australas. Universities Power Eng. Conf. (AUPEC)*, Nov. 2018, pp. 1–6.

[3] *Rotating Electrical Machines—Part 26: Effects of Unbalanced Voltages on the Performance of Three-Phase Cage Induction Motors*, document IEC 60034-26:2006.

[4] J. Faiz, H. Ebrahimpour, and P. Pillay, "Influence of unbalanced voltage on the steady-state performance of a three-phase squirrel-cage induction motor," *IEEE Trans. Energy Convers.*, vol. 19, no. 4, pp. 657–662, Dec. 2004.

[5] *Motors and Generators*, NEMA Standard Publication MG 1-1993.

[6] J. Williams, "Operation of 3-phase induction motors on unbalanced voltages," *Trans. Amer. Inst. Electr. Eng. III, Power App. Syst.*, vol. 73, no. 1, pp. 125–133, 1954.

[7] G. Bucci, F. Ciancetta, E. Fiorucci, and A. Ometto, "Uncertainty issues in direct and indirect efficiency determination for three-phase induction motors: Remarks about the IEC 60034-2-1 standard," *IEEE Trans. Instrum. Meas.*, vol. 65, no. 12, pp. 2701–2716, Dec. 2016.

[8] S. Salon, *Finite Element Analysis of Electrical Machines*. Boston, MA, USA: Kluwer, 1995.

[9] A. Jalilian, V. J. Gosbell, B. S. P. Perera, and P. Cooper, "Double chamber calorimeter (DCC): A new approach to measure induction motor harmonic losses," *IEEE Trans. Energy Convers.*, vol. 14, no. 3, pp. 680–685, Sep. 1999.

[10] *Rotating Electrical Machines—Part 2: Methods for Determining Losses and Efficiency of Rotating Electrical Machinery From Tests (Excluding Machines for Traction Vehicles), First Supplement: Measurement of Losses by the Calorimetric Method*, document IEC 34-2A, 1972.

[11] W. Orthwein, *Clutches and Brakes—Design and Selection*, 2nd ed. New York, NY, USA: Marcel Dekker, 2004.

[12] *Rotating Electrical Machines—Part 2-1: Standard Methods for Determining Losses and Efficiency From Tests (Excluding Machines for Traction Vehicles)*, document IEC 60034-2-1, Jun. 2014.

[13] T. L. Bergman, F. P. Incropera, A. S. Lavine, and D. P. DeWitt, *Introduction to Heat Transfer*. Hoboken, NJ, USA: Wiley, 2011.

PATHUM SUDASINGHE (Member, IEEE) received the B.Sc. degree in electrical engineering from the University of Moratuwa, Sri Lanka, in 2015. He is currently pursuing the Ph.D. degree in electrical engineering with the University of Moratuwa, and the University of Wollongong, Australia.

From 2015 to 2017, he was a Research Assistant with the Department of Electrical Engineering, University of Moratuwa. He is also a Joint Ph.D. Student with the University of Moratuwa and the University of Wollongong. His research interest includes development of a precise and economical derating mechanism for three-phase induction motors operating under supply voltage unbalance.

UPULI JAYATUNGA (Senior Member, IEEE) received the B.Sc. (Eng.) and M.Sc. degrees in electrical engineering from the University of Moratuwa, Moratuwa, Sri Lanka, in 2002 and 2009, respectively, and the Ph.D. degree from the University of Wollongong, Wollongong, NSW, Australia, in 2014. She is currently a Senior Lecturer with the Department of Electrical Engineering, University of Moratuwa, as well as an Honorary Fellow with the University of Wollongong. Her research interests include power quality, and power system modeling and analysis.

PHILIP COMMINS (Member, IEEE) received the B.E. degree (Hons.) in mechatronics and the Ph.D. degree in high precision tubular linear motors from the University of Wollongong, Wollongong, NSW, Australia, in 2006 and 2013, respectively. He joined the Fault Current Limiter Research Group, University of Wollongong, as a full-time Research Fellow, in 2011, focusing on the modeling, optimizing, designing, and experimentally testing saturated core fault current limiters (FCLs). His work has included extensive magnetic modeling of saturated core FCLs using 3D finite-element-analysis techniques. He joined the Electric Vehicle Research Group with an ARC Discovery Project, in 2014. Since 2017, he has been working with the Facility for Intelligent Fabrication (FIF), a collaboration between UOW, TAFE NSW, and Weld Australia, to carry out applied research in industrial automation.

JEFF MOSCROP (Member, IEEE) received the B.E. (Hons.) and Ph.D. degrees from the University of Wollongong, in 1998 and 2008, respectively.

He is currently a Senior Lecturer with the School of Electrical, Computer and Telecommunications Engineering, University of Wollongong. Since 2000, he has been involved in the design and development of complex experimental test-beds for research purposes, including linear servo-moto test beds, magnetically impelled arc butt welding test-beds and high temperature superconducting test-beds. He set-up a Fault Current Limiter Research Group, University of Wollongong, along with Australia's first dedicated FCL testing facility (which tests small and medium scale FCL designs), in 2008. He has also been directly involved in commercial FCL designs and testing of commercial FCLs.

SARATH PERERA (Senior Member, IEEE) received the B.Sc.Eng. degree in electrical power engineering from the University of Moratuwa, Sri Lanka, in 1974, the M.Eng.Sc. degree in electrical engineering from the University of New South Wales, Sydney, NSW, Australia, in 1979, and the Ph.D. degree in electrical engineering from the University of Wollongong, Wollongong, NSW, Australia, in 1988.

He was a Lecturer with the University of Moratuwa. He worked as a Professor of electrical engineering with the University of Wollongong, where he was also the Technical Director of the Australian Power Quality and Reliability Centre. He has been active in electromagnetic modeling, machine design and analysis, in particular permanent magnet machines. His current research interests include general area of power quality and in particular voltage fluctuations and flicker. He is also a member of the Standards Australia Committee on Power Electronics.